In-medium nucleon mass renormalization detected in β decays of spin aligned ^{12}B and ^{12}N

K. Minamisono, K. Matsuta, T. Minamisono, T. Yamaguchi, T. Sumikama, T. Nagatomo, M. Ogura, T. Iwakoshi, M. Fukuda, and M. Mihara
Department of Physics, Osaka University, 1-1 Machikaneyama, Toyonaka, Osaka 560-0043, Japan

K. Koshigiri
Department of Physics, Osaka Kyoiku University, 4-698-1 Asahigaoka, Kashiwara, Osaka 582-8582, Japan
(Received 2 July 2001; published 20 December 2001)

The axial charge in the weak nucleon axial vector current has been precisely determined by measuring the alignment correlation terms in the β-ray angular distributions of the purely spin aligned mirror pair nuclei ^{12}B($I^\pi=1^+, T_{1/2}=20.2$ ms) and ^{12}N($I^\pi=1^+, T_{1/2}=11.0$ ms). The axial charge was determined to be $y=4.96\pm0.09$ (stat.)±0.05 (syst.) at a 90% confidence level. The previously obtained data in the year 1996 was reanalyzed to be added to the present result. The combined result is $y=4.90\pm0.10$ at a 90% confidence level. The axial charge is enhanced as much as (72 ± 4)% from the impulse approximation model calculated value $y_{\mathrm{IA}}=2.85$. Calculations using the impulse approximation with the soft-π contribution $y_{\mathrm{th}}=4.15$ explain the data quite well but not completely. If we introduce the in-medium mass renormalization the unexplained part of the experimental result corresponds to an in nuclear-medium nucleon mass reduction of (16 ± 4)% at a 90% confidence level relative to the free nucleon mass, at the place where the decaying nucleon resides.

DOI: 10.1103/PhysRevC.65.015209 PACS number(s): 23.40.Hc, 23.40.Bw, 24.85.+p, 21.60.Cs

I. INTRODUCTION

In order to study non-nucleonic degrees of freedom in the nucleus, the axial charge matrix element is one of the best playing fields. Theoretically, Kubodera, Delorme, and Rho pointed out [1] that the axial charge matrix element, which is defined by the time like component of the axial vector current divided by the Gamow-Teller matrix element, is significantly enhanced by the meson exchange current relative to the value derived from the impulse approximation (IA). The magnitude of the enhancement in the axial charge was estimated to reach 40% of the IA value, considering the soft-π effect [2]. Measurements of the axial charge in the mass $A=12$ system shows an enhancement of as much as 60% [3,4]. Such huge mesonic effects have not yet been found in other phenomena such as the proton capture of a neutron, the photodisintegration of a deuteron and the effective g factors of nuclear magnetic moments [5]. The large size of the mesonic effects make it possible to perform detailed studies on the effect inside the nucleus in spite of the lack of complete knowledge of the nuclear structure. In 1991, Warburton *et al.* [6] showed that the axial charge matrix elements around Pb nuclei, obtained from the first forbidden β decay rates, were systematically enhanced by 80% compared with the IA value. In light nuclei the β decay rate of $^{16}\mathrm{N}(0^-) \rightarrow {}^{16}\mathrm{N}(0^+)$ also shows a 60% enhancement of the axial charge [7] which cannot be explained completely by the IA value and exchange currents. Also in the mass $A=12$ system, where a large enhancement of 60% was found, the theoretical calculation based on the IA value and the soft-π theorem was still -18% different from the experimental value [4]. The large experimental enhancements may be explained by including the heavier meson exchange currents, the renormalization of the nucleon mass and the π decay constant in the nuclear medium and a reduction of the tensor force in the effective interaction in the nucleus. One of the explanations for the large enhancement was proposed by Kirchbacha *et al.* [8], where the short-range exchange currents originating from the exchange of heavier mesons were taken into account. On the other hand, Warburton and Towner [6,9] showed by including the heavy-meson exchange currents with the short-range correlation and the hard-π model that the numerical values of the axial charge matrix elements are not so much different from those derived from the soft-π exchange current. Their analysis of the β-decay rates of the nuclei in the Pb region using a realistic nucleon-nucleon potential with a weaker tenor force gave values close to the experimental ones with a still unexplained excess of about 25%. Therefore, more precise experimental values of the light nuclei where nuclear structures and β decays are well studied are required to give a conclusive understanding on the meson exchange mechanisms and the possible in-medium mass renormalization [4]. We began measurements in the year 1980 to determine an accurate value of the axial charge by measuring the alignment correlation terms in the mass $A=12$ system. We not only improved the experimental technique but also studied all the possible systematic errors that may cause some effect in the extraction of the results [3,4]. Parallel to the recent experimental progress, theoretical calculations have been made on the relevant refined nuclear structures and wave functions of leptons in the β-decay process [10,11]. The latest value of the axial charge from the alignment correlation experiment in the mass $A=12$ system [4] is $y=4.66\pm0.06$ (stat.)±0.13 (syst.) in 1σ level. The result, however, has a large systematic error coming from the uncertainty in evaluating the converted alignments. The detected alignment terms have a spurious effect caused by the intensity fluctuation of the incident production beam in the positive and the negative alignment creation cycles. In the present study the large systematic error was eliminated by use of a newly developed timing program for the measurement of the alignment correlation terms.

II. NUCLEAR β DECAY

A. Interaction Hamiltonian

Weak nuclear processes are described with the well-known current-current-type *V-A* interaction [11] as $H_I = \sqrt{1/2}(V_\lambda + A_\lambda)\{\overline{\psi}_e \gamma_\lambda (1+\gamma_5)\psi_\nu\} + \text{H.c.}$, where V_λ and A_λ are the vector and the axial vector currents, respectively. Due to the strong interaction in the nucleus, Lorenz invariance allows for several other currents. As a result, the most general forms of the vector and the axial vector currents made up of the Dirac matrices γ_λ as well as the four-momentum transfer k_λ are given by

$$V_\lambda = \overline{\psi}_p (f_V \gamma_\lambda + f_W \sigma_{\lambda\rho} k_\rho + i f_S k_\lambda)\psi_n, \tag{1}$$

$$A_\lambda = \overline{\psi}_p \gamma_5 (f_A \gamma_\lambda + f_T \sigma_{\lambda\rho} k_\rho + i f_P k_\lambda)\psi_n, \tag{2}$$

with $\sigma_{\lambda\rho} = [\gamma_\lambda, \gamma_\rho]/2i$ and $k_\lambda = k_p - k_n$. Along with the main vector f_V and the main axial vector f_A currents, four other currents are included in the representation. They are the weak magnetism f_W, the induced scalar f_S, the induced tensor f_T, and the induced pseudoscalar f_P currents. The form factors are real if time-reversal invariance holds and generally they are the functions of k^2. The structure of the weak nucleon currents is characterized by the magnitudes of those six form factors in the vector and the axial vector currents and is well described in Ref. [12].

B. β-ray angular distribution from oriented nuclei

A theory of nuclear β decay was formulated by Morita *et al.* [10,13] in which higher order corrections such as the Coulomb correction for the finite size of the nucleus and higher partial waves of the lepton wave function were properly taken into account. For the present experiment it is necessary to employ a formalism with these corrections since we are concerned with the small recoil terms in the β decay. The β-ray angular distribution for the mass $A=12$ of ^{12}B and ^{12}N decaying into the ground state in ^{12}C, that is, $(I^\pi, T, T_z : 1^+, 1, \mp 1) \rightarrow (0^+, 0, 0)$, from oriented nucleus is given by

$$\frac{dW}{dE\, d\Omega} \propto pE(E_0 - E)^2 B_0(E)\left(1 + P\frac{B_1(E)}{B_0(E)}P_1(\cos\theta) + A\frac{B_2(E)}{B_0(E)}P_2(\cos\theta)\right), \tag{3}$$

where $E(E_0)$ is the β-ray energy (endpoint energy), θ is the angle between the polarization direction and the direction of the emitted β ray, p is the electron momentum, P_i is the Legendre polynomials, B_1/B_0 is the polarization correlation term, and B_2/B_0 is the alignment correlation term. Here, the radiative or other corrections to the ratio B_i/B_0 are negligible as studied by Yokoo *et al.* [14]. These P and A are the degree of the nuclear spin polarization and the nuclear spin alignment, respectively, which are defined as $P = a_{+1} - a_{-1}$, $A = 1 - 3a_0$ with $a_{+1} + a_0 + a_{-1} = 1$ for nuclear spin $I=1$ where a_i are the magnetic substate populations. Neglecting higher order terms in the IA the alignment correlation term is simply described as

$$\frac{1}{E}\frac{B_2(E)}{B_0(E)} = \frac{2}{3}\left\{ \pm\left(a - \frac{f_T}{f_A}\right) - \frac{y_{\mp}}{2M}\right\}, \tag{4}$$

where M is the nucleon mass and the subscript $\mp$ refers to electron or positron decays. The first term a in Eq. (4) is due to the weak magnetism and is given by the strong form of the conserved vector current (CVC) theory [15,16]. The third term is the ratio of the timelike component in the main axial vector current, also called the axial charge, and the main axial vector current $y = -2M\int i\gamma_5 \mathbf{r} / \int \boldsymbol{\sigma}$. Thus, the correlation coefficient contains the weak magnetism term, the coefficient of the induced tensor term, and the axial charge. From the sum of the alignment correlation term given in Eq. (4) between ^{12}B and ^{12}N, the axial charge $y = [y_-(^{12}B) + y_+(^{12}N)]/2$, can be extracted as

$$\left[\frac{1}{E}\frac{B_2(E)}{B_0(E)}\right]_{^{12}\text{B}} + \left[\frac{1}{E}\frac{B_2(E)}{B_0(E)}\right]_{^{12}\text{N}} = -\frac{2}{3}\frac{y}{M}. \tag{5}$$

On the other hand, the difference gives the induced tensor form factor as

$$\left[\frac{1}{E}\frac{B_2(E)}{B_0(E)}\right]_{^{12}\text{B}} - \left[\frac{1}{E}\frac{B_2(E)}{B_0(E)}\right]_{^{12}\text{N}} = \frac{4}{3}\left(a - \frac{f_T}{f_A} + \frac{\Delta y}{2M}\right), \tag{6}$$

where Δy is the possible asymmetry in the axial charge which is defined as $\Delta y = [y_+(^{12}N) - y_-(^{12}B)]/2$. The induced tensor form factor is one of the important keys to test the *G*-parity symmetry in the weak nucleon current as well as to know how close we can get to the fundamental level of the nuclear β decay as a direct decay of the quark inside the nucleus. A detailed discussion on this subject can be seen elsewhere [16,17].

III. EXPERIMENT

The ^{12}B and ^{12}N nuclei were produced at the Osaka University 4.75-MV Van de Graaff accelerator. The reaction chamber and part of the experimental apparatus are shown in Fig. 1. All the components of the experimental equipment other than counter telescopes and the electromagnet were contained in a steel vacuum chamber (not shown in the figure). Part of the chamber was made of plastic to reduce scattered β rays. The energy of the scattered electrons is very much reduced (~ 4 MeV) by the plastic before reaching the β-ray counters even if electrons scattered by the steel wall. The experimental procedure consisted of four steps. These steps are summarized in the following sections. Section III A: production of the polarized nuclei, Sec. III B: recoil implantation into the Mg catcher, Secs. III C and III D: spin manipulation from polarization to alignment, and Sec. III E: β-ray detection of the aligned nuclei.

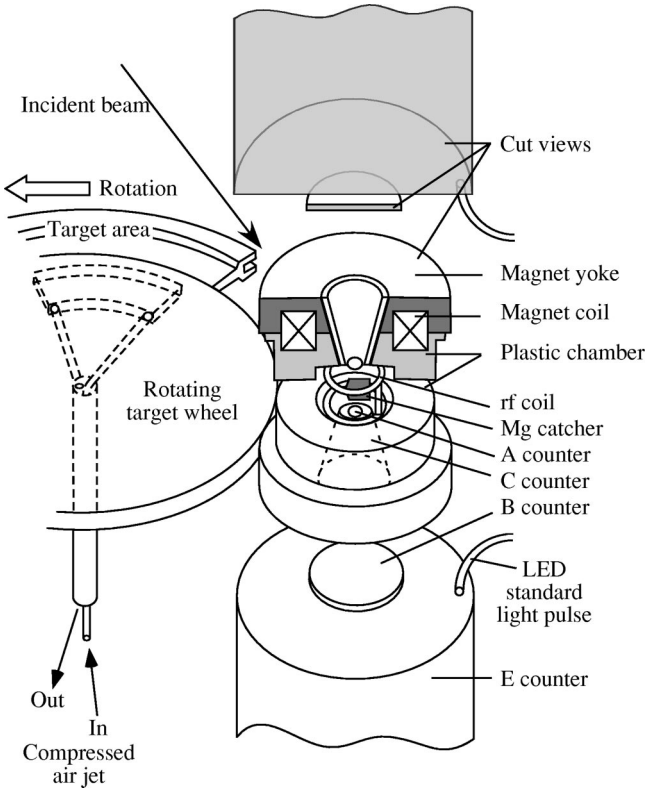

FIG. 1. Main part of the reaction and NMR chamber. The vacuum chamber is not shown in the figure. The part of the chamber close to the β-ray path to the counter system is made of plastic to reduce the scattered β rays. The target ribbon is attached to the rotating target system (target area), which rotates at a period of 75 ms. ^{12}B(^{12}N) produced through the nuclear reaction is implanted into Mg catcher and the β rays from the stopped nuclei are detected by the counter telescopes placed above and below the catcher.

A. Production of ^{12}B and ^{12}N

The ^{12}B (^{12}N) nuclei were produced through the nuclear reaction ^{11}B$(d,p)^{12}$B [^{10}B$(^3$He$,n)^{12}$N]. A 1.5 MeV deuteron (3.0 MeV ^{3}He) beam provided by the 4.75-MV Van de Graaff accelerator at Osaka University was used to bombard a ^{11}B(98.0%; ^{10}B 2.0%) [^{10}B(90.4%; ^{11}B 9.6%) or ^{10}B(99.8%; ^{11}B 0.2%)] enriched reaction target (300 μg/cm^2) evaporated on a 0.15-mm-thick Mo backing ribbon (430$\times$3.2 mm) attached to a rotating target holder with the grazing angle of 10° relative to the incident beam direction. The target, withstanding currents up to 30 μA, was cooled from inside the holder by a compressed air jet. A typical counting rate of β rays from stopped ^{12}B (^{12}N) in the Mg catcher detected by two sets of counter telescope was 4 kcps (200 cps) at a beam intensity of 15 μA (30 μA). The target wheel rotated at a frequency of 75 ms. The Mo target ribbon was attached to one third of the circumference of the target wheel as illustrated in Fig. 1. The pulsed incident beam was synchronized to the rotation of the target wheel so that we had the beam on target for 25 ms. During the beam-off time (50 ms), the target wheel was hidden in a radiation shield to avoid background radiation from the target, and during this time the β-ray counting and the spin manipulation were performed.

B. Recoil implantation

The produced ^{12}B (^{12}N) were ejected at a recoil angle 40°–75° (20°–55°) which was chosen by the target groove and the effective area of the catcher so that maximum polarization was obtained. The nuclei were then implanted into a recoil catcher of Mg single crystal (hcp) placed under an external magnetic field of $H_0=600$ Oe applied parallel to the direction of the polarization. The typical size of the catcher was 15 mm $\times$ 20 mm in area and 500 μm in thickness. The maximum recoil energy of ^{12}B (^{12}N) was 0.44 MeV (1.5 MeV), and the maximum implantation depth in the catcher was 1.5 μm (2.7 μm). The energy spread caused by the nuclear reaction and the target thickness, resulted in an implantation depth in the catcher distributed almost uniformly from the surface to the maximum depth. The polarization created through the nuclear reaction was about 10% (20%) and a small alignment of 2% (3%) was also produced. The degree of polarization produced was measured with the β-NMR (nuclear magnetic resonance) technique by detecting the asymmetric β-ray distribution relative to the polarization direction with a set of plastic scintillation counter telescopes placed above (up) and below (down) the catcher relative to the direction of the polarization axis.

C. Spin manipulation

1. Principle of the spin manipulation

The polarization resulting from the nuclear reaction was artificially converted into the alignment with, ideally, no residual polarization. By the use of spin manipulation, we were able not only to produce a large alignment compared with the small initial alignment produced through the nuclear reaction technique but we were also able to create both positive and negative alignments. In this technique we use NMR with a magnetic interaction between the magnetic moment μ of ^{12}B(^{12}N) and an external magnetic field H_0 superposed on the electric interaction between a quadrupole moment Q of ^{12}B(^{12}N) and the electric field gradient q in the Mg single crystal. The crystal c axis of the Mg catcher was placed parallel to H_0. The interaction Hamiltonian is written as $H_I = H_M + H_E$, where

$$H_M = -\mu H_0,$$

$$H_E = \frac{eqQ}{4I(2I-1)}\left\{3I_Z^2 - I(I+1) + \frac{\eta}{2}(I_+^2 + I_-^2)\right\}. \quad (7)$$

Here, I is the nuclear spin of the implanted nucleus, eqQ/h is the quadrupole coupling constant, and I_+ (I_-) is the raising (lowering) operator of the magnetic substate m. For ^{12}B and ^{12}N in the Mg crystal, the electric field gradient is symmetric around the crystal c axis so that the asymmetry parameter η of the electric field gradient is zero $\eta = (V_{XX}\text{-}V_{YY})/V_{ZZ} = 0$ [18]. Here the electric field gradient is defined by the principal components of $V_{ii} = d^2V/dX_i\,dX_i$ as $|V_{XX}| \leqslant |V_{YY}| \leqslant |V_{ZZ}|$ and $V_{ZZ} = q$. In the first-order perturbation calculation, the energy levels E_m for the magnetic substates m are unequally split because of the quadrupole interaction

$$E_m = -h\nu_L m + \frac{h\nu_Q}{6}\left(\frac{3\cos^2\beta - 1}{2} + \eta\sin^2\beta\cos 2\gamma\right) \times\{3m^2 - I(I+1)\},$$

$$\nu_Q = \frac{3eqQ}{2I(2I-1)h}. \quad (8)$$

Here, ν_L is the Larmor frequency and β and γ are the polar angles between the principal axis of the electric field gradient and the external magnetic field. In the present experimental condition $\beta = 0°$ and $\eta = 0$, the energy splits between the magnetic substates $m = 1 \leftrightarrow 0$ denoted F_H as a corresponding resonance frequency, and between substates $m = 0 \leftrightarrow -1$ denoted F_L are well separated so that a specific transition between selected substates can be induced. Here the resonance frequencies are given in a first-order perturbation calculation by $F_H = \nu_L - \nu_Q/2$ and $F_L = \nu_L + \nu_Q/2$. The quadrupole coupling constant in Mg is known [18] to be $eqQ/h = -(47.0 \pm 0.1)$ kHz for ^{12}B and $eqQ/h = -(59.3 \pm 1.7)$ kHz for ^{12}N. The alignment was created from the polarization by use of spin manipulation. For the spin manipulation, two types of rf applications were used. One is an adiabatic fast passage (AFP) field denoted by $\vec{F}_L$ and $\vec{F}_H$, which interchanges the populations of two specific magnetic substates. The other is a depolarization (dep) field denoted by $\overline{F_L}$ and $\overline{F_H}$, which equalizes the populations of two specific magnetic substates. Applying a set of rf fields, the population in the unequally separated magnetic substates are equalized and/or interchanged so that the positive and the negative alignment are produced.

2. Timing program for the creation of alignment

The spin manipulation for the artificial creation of the alignment and β-ray detection were performed in accordance with the timing programs controlled by a microcomputer. There were two types of newly developed timing programs used in this experiment. One was a timing program named the ''main sequence program'' for the creation of the positive and the negative alignment and the measurement of β-ray energy spectra from the aligned nuclei. The other was a timing program named the ''test sequence program'' in which the efficiency of the spin manipulation was checked. Each program consisted of several production beam cycles synchronized with the rotating target.

a. Main sequence program. A set of main sequence program processed four kinds of beam cycles which are illustrated in Fig. 2. The $A_M^{\pm}$ and $A_M^{\mp}$ cycles for the production of the positive and negative alignment were the principal part of the experiment and measured the β-ray spectra from the aligned nuclei. In the $A_M^{\pm}$ cycle, by applying a depolarizing field $\overline{F_H}$ before counting Sec. I and sequentially applying an AFP field $\vec{F}_L$ before counting Sec. II, we obtained the positive alignment in Sec. II. To confirm the alignment in Sec. II, the alignment was converted back again into the polarization in Sec. III. Right after counting Sec. III, alignment with the opposite sign was produced in counting Sec. V. To start from the negative alignment in another beam cycle of $A_M^{\mp}$, we replaced the $\overline{F_H}$ and $\vec{F}_L$ rf set with the $\overline{F_L}$ and $\vec{F}_H$ rf set. The typical result of the polarization change in $A_M^{\pm}$ and $A_M^{\mp}$ as a function of time are illustrated in Fig. 3. The alignments were successfully created in Secs. II and V. The other part of the main sequence program were the P_M^+ and P_M^- cycles for the measurement of the geometrical center. These cycles were performed to determine the counting rate ratio g corresponding to zero polarization. As shown in Fig. 2 the time dependent decay of the polarization produced through the nuclear reaction was measured in the P_M^+ cycle with no rf, while in the P_M^- cycle the time dependent decay of the inverted polarization created by $\vec{F}_H$-$\vec{F}_L$-$\vec{F}_H$ rf was measured. A set of the main sequence program consisted of 20 pairs of $A_M^{\pm}$ and $A_M^{\mp}$ cycles, which were followed by 10 pairs of P_M^+ and P_M^- cycles. The set was repeated until a preset counting statistics were obtained. An ideal spin manipulation yields the alignment as $A_{\rm II}^{\pm} = (\pm 3P_0 - A_0)/2$ and $A_{\rm V}^{\pm} = (\pm 3P_0 - A_0)/4$ where P_0 is the initial polarization, A_0 the initial

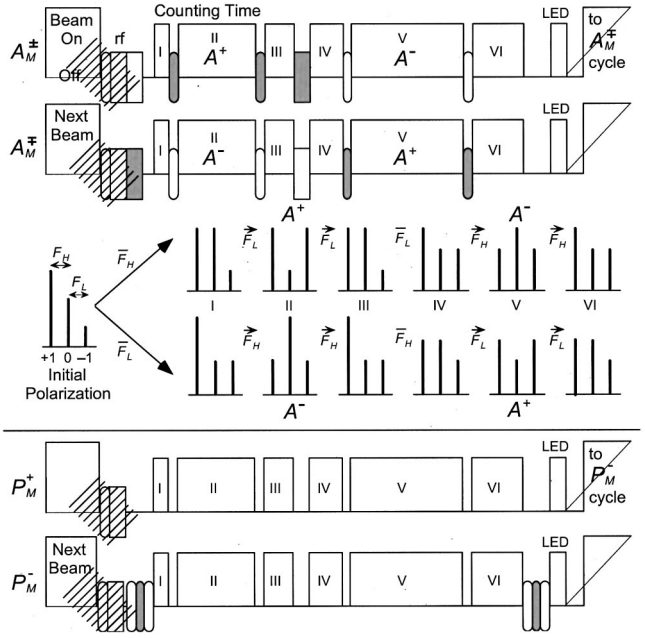

FIG. 2. New timing program (main sequence program) and magnetic substates populations. The main sequence program is illustrated in which positive and negative alignment are produced. The regions labeled from I to VI are the counting times. The squares and the ellipses between the counting times represent the rf for spin manipulation. The rf hatched with gray represents the production of positive alignment, white represents negative alignment, and hatched by lines the destruction of the second component. The $A_M^{\pm}$ and $A_M^{\mp}$ cycles are shown in the upper part of the figure together with the change of the magnetic substates populations by the spin manipulation. After the spin manipulation by use of the NMR technique was completed following the end of the production time, β ray counting was started. In the lower part the P_M^+ and P_M^- cycles are shown from which g was determined. A set of main sequence program consisted of 20 pairs of $A_M^{\pm}$ and $A_M^{\mp}$ cycles, which were followed by 10 pairs of P_M^+ and P_M^- cycles. The sets were repeated until the preset counting statistics were obtained.

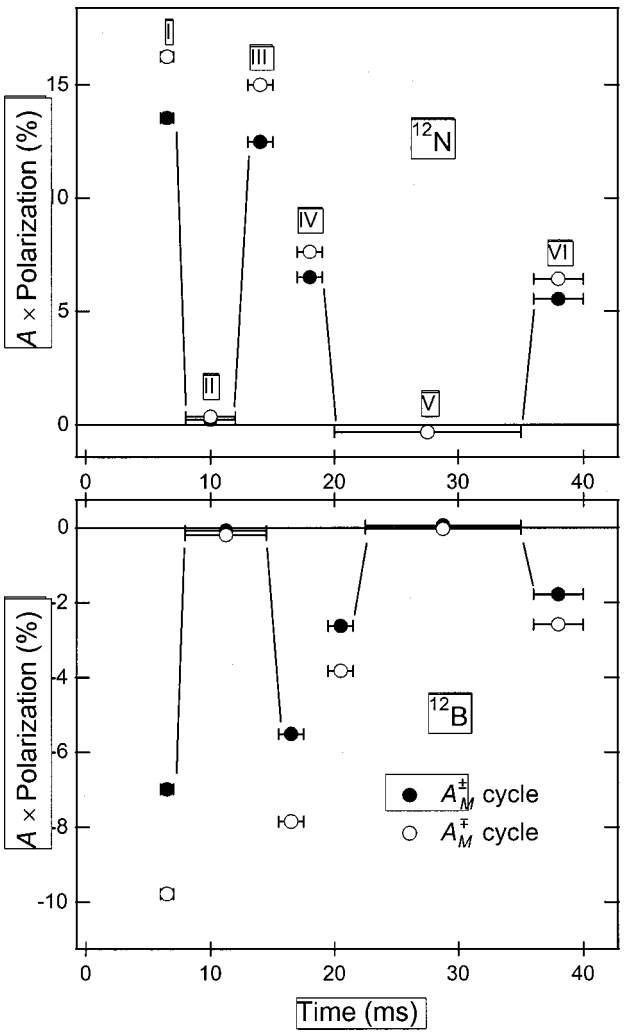

FIG. 3. Typical result of the spin manipulation in the Main sequence program. The upper part of the figure is the result of ^{12}N and the lower part of ^{12}B. A in the ordinate is the asymmetry parameter (-1 for ^{12}B and $+1$ for ^{12}N). The full circles are for the polarization change in the $A_M^{\pm}$ cycle and the open circles in the $A_M^{\mp}$ cycle. The lines in the figure schematically illustrate the change of the polarization by the spin manipulation. At time zero the incident beam was chopped. The alignments were successfully created in Secs. II and V. The smaller polarization in $A_M^{\pm}$ cycle relative to that in the $A_M^{\mp}$ cycle is due to the initial alignment produced through the nuclear reaction.

TABLE I. Result of the spin manipulation.

	^{12}B	^{12}N
P (%)	11.25 ± 0.01	20.12 ± 0.06
α (%)	-94.8 ± 0.04	-94.9 ± 0.09
η(LF) (%)	98.13 ± 0.08	99.1 ± 0.3
η(HF) (%)	98.29 ± 0.07	99.1 ± 0.3
$\hat{A}$ (%)	39.99 ± 0.06	84.2 ± 0.4
ΔP (%)	-0.09 ± 0.01	0.28 ± 0.05
$T_1(P)$ (ms)	78.1 ± 0.4	247 ± 3
$T_1(A)$ (ms)	30.4 ± 0.3	75 ± 8

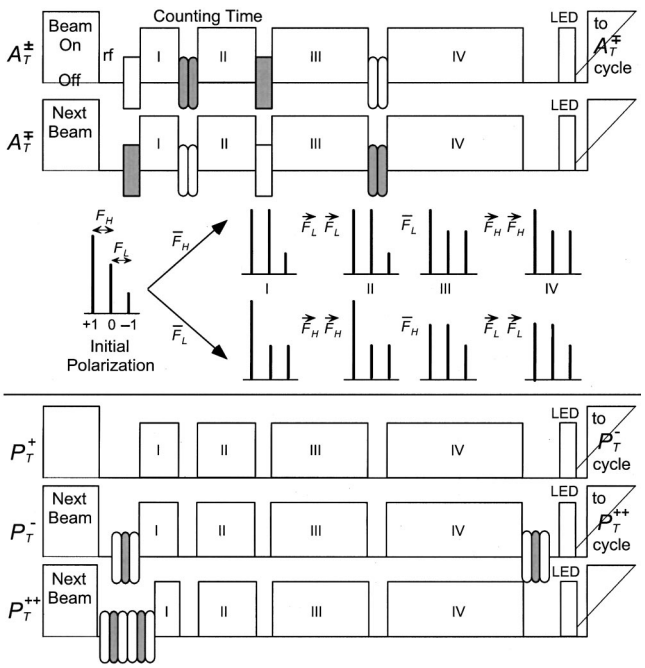

FIG. 4. New timing program (test sequence program) and magnetic substates populations. The test sequence program is illustrated in which the efficiency of the spin manipulation was measured. The regions labeled from I to IV are the counting times. The squares and the ellipses between the counting times represent the rf for spin manipulation. The rf hatched with gray represents the production of positive alignment and white represents negative alignment. The $A_T^{\pm}$ and $A_T^{\mp}$ cycles are shown in the upper part of the figure together with the change of the magnetic substates populations by the spin manipulation. In the lower part the P_T^+, P_T^-, and P_T^{++} cycles are shown from which the geometrical center g and the spin lattice relaxation time T_1 were determined. The test sequence program was performed for an hour (two hours) in every 5 h (10 h) run of the main sequence program in ^{12}B (^{12}N) experiment.

alignment produced through the nuclear reaction and $A_i^{\pm}$ is the alignment created in Sec. I. The difference of the positive and the negative alignment becomes 4.5 times larger than the initial polarization $\hat{A}=(A_{\rm II}^+-A_{\rm II}^-)+(A_{\rm V}^+-A_{\rm V}^-)=4.5P_0$, which reached actual values of 40% for ^{12}B and 85% for ^{12}N as listed in Table I. This large effective alignment makes the experiment very efficient and reliable.

b. Test sequence program. Though an ideal spin manipulation yields the difference of the positive and the negative alignment to $\hat{A}=4.5P_0$, actually $\hat{A}$ varied from the ideal amount because of the imperfect efficiency of the spin manipulation. To determine the true alignment, the efficiency for the interchange of two specific populations of magnetic states ($a_i \leftrightarrow a_{i+1}$) had to be measured in a set of the test sequence program. As shown in Fig. 4 five kinds of beam cycles were used for this determination. They were $A_T^{\pm}$ and $A_T^{\mp}$ cycles for the measurement of the degree of achievement of spin manipulation for the creation of the positive and the negative alignment, respectively. The procedure of the test sequence program was the same as that of the main sequence program except for the absence of counting Secs. II and V, where the β-ray energy spectrum from the aligned nuclei

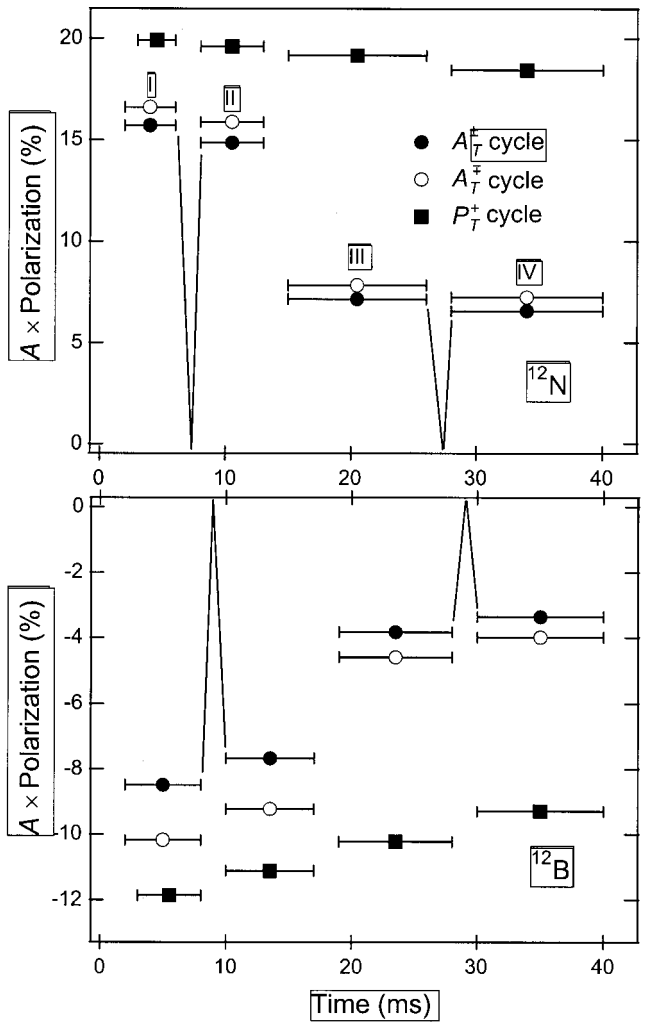

FIG. 5. Result of the spin manipulation in test sequence program. The upper part of the figure is for ^{12}N and the lower part for ^{12}B. A in the ordinate is the asymmetry parameter (-1 for ^{12}B and $+1$ for ^{12}N). The full circles are for the polarization change in the $A_T^{\pm}$ cycle and the open circles in the $A_T^{\mp}$ cycle. The lines in the figure schematically illustrate the change of the polarization by the spin manipulation. An alignment was created between the counting Secs. I and II (III and IV) and immediately converted back to polarization. The difference of the polarization between Secs. I and II (III and IV) is due to the efficiency of the manipulation and to the T_1. The full squares are for the polarization change in the P_T^{+} cycle in which no rf was applied for the measurement of T_1.

were measured. Right after the alignment was produced, the alignment was immediately converted back again to polarization. Thus, the deviation between the initial and the final polarization represents the achievement of the applied rf field and T_1. A typical result of the polarization change as a function of time in the test sequence program is illustrated in Fig. 5, where part of the beam cycles are shown. In addition, P_T^{+}, P_T^{-}, and P_T^{++} cycles measured g and T_1 by detecting the time dependent decay of the initial polarization. The test sequence program was performed for 1 h (2 h) in every 5 h (10 h) run of the main sequence program in ^{12}B (^{12}N) experiment. The results of spin manipulation are summarized in Table I. In the table P is the initial polarization produced through the nuclear reaction, α the efficiency of the spin inversion defined by the inverted $P'=\alpha P$, $\eta(F_L)$ the efficiency for creation of the positive alignment, $\eta(F_H)$ the efficiency for creation of the negative alignment and T_1 the spin lattice relaxation time.

D. Mg catcher

A catcher was cut out from a bulk Mg single crystal so that the c axis was in the plane of the catcher. For the cutting, a spark slicer was used to minimize the damage on the sliced crystal. In the next step, the surface of the sliced crystal, the catcher, was etched by 50 μm at room temperature with citric acid (5% concentration) to a thickness of about 500 μm, to remove damages and defects on the surface produced by the slicing process. After the etching the residuals on the surface were quenched by deionized water and the water was blown off by a jet of dry N_2 gas. The x-ray diffraction pattern of the crystal was checked to confirm the orientation of the c axis and the structure near the surface. The Mg catcher was mounted on the tip of an Al holder of 0.5 mm in thickness which was attached on the coil holder along with an rf coil. The backing was cooled by water flow to prevent heating due to irradiation of the production target and from eddy currents created by the rf fields. During the experiment, the surface of the catcher slowly became contaminated by the sputtered target due to beam irradiation. This resulted in a gradual decrease in the measured polarization as used. To remove the contamination and to recover the polarization, the surface of the Mg catcher was etched every 72 h. For reliable spin manipulation accurate knowledge of the quadrupole interaction is very important. We found a new minority location of ^{12}B and ^{12}N in Mg (second component) [18] which might affect the result of the spin manipulation and, in the worst case, would have about 15% of population relative to the population of the well known majority location (main component). From detailed studies, it has been shown that (1) the second component is caused by micrograins introduced into the crystal during the growth process and/or of the cutting and treatment of the crystal, (2) the c axis of the micrograin is perpendicular to that of the bulk crystal, and (3) the absolute value of the electric field gradient for the second component is the same as that for the main component and perpendicular to the c axis of the bulk crystal. The coupling constant for the second component is $eqQ/h \sim -45$ kHz for ^{12}B and $eqQ/h \sim -60$ kHz for ^{12}N with q vertical to the c axis of the bulk crystal. The amount of the second component is strongly dependent on the way the Mg catcher is treated. Thus, in the present experiment a spark slicer was used for the cutting out a catcher and its surface was etched. Every time a newly treated catcher was used the amount of the second component was shown to be zero $P=0$ within the experimental error by detecting the NMR signal from that component. To ensure the absence of the effects from the second component in the final result, we destroyed the polarization of the second component by applying a set of rf fields before each measurement of the energy spectra as illustrated in Fig. 2. Moreover, since the crystal c axis of Mg

catcher was placed parallel to the external magnetic field, the two set of resonance frequencies resulting from the main and the second component were well separated. Thus the spin manipulation for the main component was not affected by the second component at all.

E. β-ray energy spectrum

1. β-ray detectors

The β rays from aligned ^{12}B and ^{12}N in Secs. II and V were detected with a 150 mm$\phi\times$175 mm plastic scintillation counter named the *E* counter. The counter was large enough to measure the entire β-ray energy and was placed above (up) and below (down) the catcher relative to the polarization direction. The counter system telescope is shown in Fig. 1. The solid angle of each telescope (1.4×10^{-2} sr/4π) was defined by two sets of thin plastic scintillation counters named the *B* counter (55 mm$\phi\times$1 mm) placed right in front of the *E* counter and a counter named the *A* counter (12 mm$\phi\times$0.5 mm), which was placed close to the catcher. The cone shaped plastic scintillation veto counter named the *C* counter was used to reject unwanted β rays scattered by the return yokes of the air core β-NMR magnet. To prevent the photomultiplier tubes (PMTs) of the *E* counter from saturation due to the prompt radiation during production time, the high voltage fed to the first dynode of the PMTs was dropped during beam-on time so as not to amplify those photoelectrons. Using this method we were able to avoid unwanted effects in the β-ray counting time. Because of the long data acquisition time (several weeks), the stability of the energy counter system had to be very high for the accurate determination of the alignment correlation terms. In the experiment, a pulse-height-gain stabilizer was used in the amplifier system. A standard light pulse from an LED pulser maintained at a constant temperature was used at the end of every beam cycle to ensure the stability of the *E* counter, as illustrated in Figs. 2 and 4. The stability of the counter system was monitored by the change in the center of gravity of the β-ray energy spectrum and was found to be within $\pm1\%$ for both the ^{12}B and ^{12}N experiments. This stability was sufficient for the precise measurement of alignment correlation terms. The small time dependent energy shift was properly taken into account as a systematic error as discussed later.

2. Trigger signal

Real events were selected by the trigger signal $A\cap B\cap\overline{C}\cap E$ in the coincidence unit. Furthermore, two signals arriving within the timing interval of 500 ns were rejected as pile-up events. The signals from these rejected events were consistent with back-scattered β rays or cosmic rays. The resultant events were further inhibited during the 10 μs busy time of the ADC. All the discriminators were inhibited during beam on time and rf time.

3. Linear signal

To ensure as high a counting rate as possible the linear signals obtained from the dynode of the PMT (HAMAMATSU R1250) of an *E* counter had a relatively short decay constant of about 1 μs and were further shortened by the delay line clipping method to about 500 ns. After the clipping they were selected by the trigger signals mentioned above to reject all the unwanted events. The selected true events were digitized by the ADC after being amplified. The spectrum data were finally read out through a CAMAC crate controller. The linear signals which originated from LED standard light pulser were led to the gain stabilizer loop. The gain shift of the system detected by the change of pulse height of the LED light was fed back to the amplifier so as to cancel the gain shift.

4. Counter response function

The β-ray energy spectrum from unoriented nuclei is given as

$$S(E)=pE(E_0-E)^2F(\pm Z,E)[1+R_0(E,E_0)], \qquad (9)$$

where $F(\pm Z,E)$ is the Fermi function and $R_0(E,\ E_0)$ the radiative correction. The measured β-ray spectra, however, varied from the shape given by $S(E)$ because of the response of the β-ray counter. β rays in the plastic scintillation counter lose kinetic energy by electric excitation in the plastic and by the bremsstrahlung process. Since the energy deposition by the monochromatic β ray in the plastic has a low energy tail in the pulse height spectrum because a part of the bremsstrahlung may escape from the surface of the counter without depositing its energy in the counter and also has a high energy tail because of the positron annihilation, a simple minded theoretical response function does not reproduce the lower energy tail and the shape at the higher energy tail at all. Scattered β rays in the Mg catcher also contributed to the lower energy tail. Thus in the present analysis the character of the monochromatic β-ray energy deposition was studied based on Monte Carlo simulation of the electromagnetic cascade shower EGS4 [19]. The response function $R(x,E)$ of β ray with monochromatic energy *E* is dependent upon the energy deposit function $f(y,E)$ which was simulated using the EGS4 code taking into account the geometry of the counter system and the NMR chamber and the effects of annihilation gamma in flight and also the one or two photon escape in scintillator were taken into account. The response function is given by the energy deposit function convoluted with the counter resolution

$$R(x,E)=\int f(y,E)\frac{1}{\sqrt{2\pi}\sigma}\exp\left[-\frac{(x-y)^2}{2\sigma^2}\right]dy. \qquad (10)$$

Here x is the observed energy, y the energy deposit, and σ the resolution of the counter, where σ is expected to have the form $\sigma_0\sqrt{E}$ and σ_0 is a constant. In Fig. 6, a part of the results of the simulations is shown. In the figure, $f(y,E)$ in the upper part and $R(x,E)$ in the lower part are shown for electrons and positrons, where the incident energy of the β rays are $E=5$, 8, and 11 MeV for electrons and $E=5$, 8, 11, and 14 MeV for positrons. Thus, the observed energy spectrum $W(E)$ is given by the statistical shape $S(E)$ in Eq. (9) convoluted with the response function

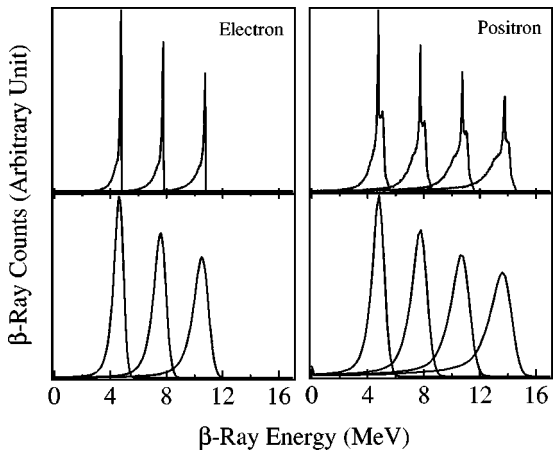

FIG. 6. Energy deposit functions $f(y,E)$ in the upper part and response functions $R(x,E)$ in the lower part are shown for electrons and positrons. The incident energy of the β rays are $E=5$, 8, and 11 MeV for electrons and $E=5$, 8, 11, and 14 MeV for positrons. For the convolution of the counter resolution $\sigma_0=0.12$ was used.

$$W(E)=\int S(\mu)R(E,\mu)d\mu, \tag{11}$$

where E is the observed energy and μ the incident energy. The reliability of the simulation was checked by measuring monochromatic β^+ and β^- rays using a spectrometer. From the experimental check, we fined $(0\pm20)\%$ difference at the lower energy tail of the shape of the experimental response function and that of simulated one, which was taken into account in evaluating a systematic error. The obtained simulated energy spectrum was used for the least χ^2 fitting to the measured energy spectra. A typical result of the fitting is shown in Fig. 7. The fitting parameters were the zero energy channel, the endpoint channel, and the normalization of the amplitude. In this fit, the counter resolution $\sigma_0=0.12$ MeV^{-1} for the up counter system and $\sigma_0=0.08$ MeV^{-1} for the down counter system were used. These values were determined by fitting the simulated energy spectrum to another set of experimental data obtained for the determination of the resolution. We found excellent agreement between the simulated spectrum and the experimental data.

5. Energy calibration

The energy scale was determined by measuring the end-point energies of β-ray spectra from several β emitters produced through nuclear reactions. For the ^{12}B experiment, ^{12}B ($E_{\rm end}=13.369$ MeV), ^{20}F ($E_{\rm end}=5.390$ MeV), and ^{28}Al ($E_{\rm end}=2.863$ MeV) were produced and measured. For the ^{12}N experiment, ^{12}N ($E_{\rm end}=16.3161$ MeV), ^{30}P ($E_{\rm end}=3.210$ MeV), and ^{15}O ($E_{\rm end}=1.732$ MeV) were produced and measured. In the extraction of the end-point energy, the least χ^2 fitting of the simulated energy spectrum was performed in which the free parameters were the zero-point energy, the end-point energy, and the normalization factor.

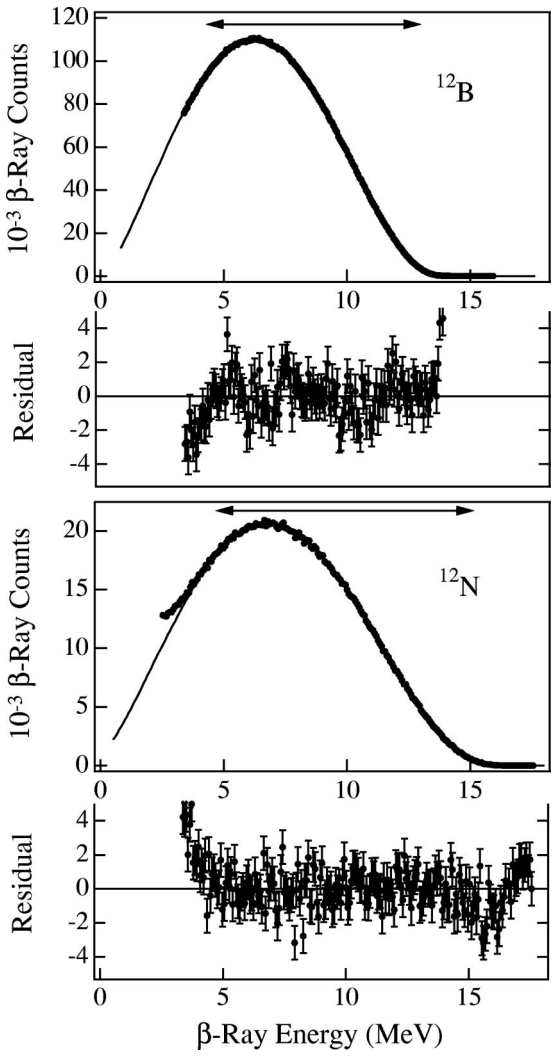

FIG. 7. β-ray energy spectrum of ^{12}B and ^{12}N. The upper part shows a typical energy spectrum of ^{12}B and the lower part ^{12}N. The dots are the experimental data and the solid lines are the best fit of the simulated energy spectrum to the data. Together with the spectrum the residuals $(N_{\rm exp}-N_{\rm fit})/N_{\rm exp}^{1/2}$, are plotted, where $N_{\rm exp}$ and $N_{\rm fit}$ are the experimental data and the fit result, respectively. The errors are from the experimental data. The fitting regions were 4.1–13.0 MeV for ^{12}B and 4.6–15.1 MeV for ^{12}N indicated by arrows. For this typical spectrum we had $\chi^2/\nu=1.29$ for ^{12}B and $\chi^2/\nu=1.00$ for ^{12}N.

IV. ANALYSIS

A. Principle of the extraction of B_2/B_0

The alignment correlation term can be extracted from the β-ray counting ratio of positively and negatively aligned nuclei for a given β-ray energy $\hat{E}_i=E_i\pm\Delta E$. In this analysis, E_i ranged from 5 to 13 MeV in total energy for ^{12}B and from 5 to 15 MeV in total energy for ^{12}N and $\Delta E=0.5$ MeV. The double ratio of up or down counters in Secs. II and V in the main sequence program is defined by

TABLE II. Correction to the alignment correlation terms and systematic errors. Corrections indicated by an asterisk have contributions both from the energy independent and dependent part. In the table the values of energy independent part multiplied by the dependent part $C(E)$ are shown, where E is the β-ray total energy. The values of the systematic errors are given in relative % to the alignment correlation coefficient and the absolute values of the total systematic errors are shown in the last row.

	^{12}B		^{12}N	
Correction	C	Error (%)	C	Error (%)
Solid angle	1.054	0.33	1.055	0.36
$\langle p/E \rangle$	0.997	<0.01	0.998	<0.01
Polarization correlation term	1.001	0.01	0.974	0.02
Alignment calculation		0.08		0.24
Energy calibration		0.50		0.50
Beam position		0.80		0.20
Catcher thickness		0.29		0.28
Decay branch*	$0.988C_{\rm BR}(E)$	0.03	$0.977C_{\rm BR}(E)$	0.03
Counter response*	$C_{\rm res}(E)$	0.80	$C_{\rm res}(E)$	0.81
HD^+ admixture*			$0.990C_{\rm HD}(E)$	0.13
Sum		1.31		1.11
Total systematic error in alignment correlation coefficient $(1/2M)$		<0.01		0.06

$$R_{U\mathrm{or}D}(\hat{E}_i)=\left[\frac{T^{\pm}N_{\rm II}^{+}(\hat{E}_i)}{T^{\mp}N_{\rm II}^{-}(\hat{E}_i)}\times\frac{T^{\mp}N_{\rm V}^{+}(\hat{E}_i)}{T^{\pm}N_{\rm V}^{-}(\hat{E}_i)}\right]_{U\mathrm{or}D}$$
$$=\left[\frac{B_0(\hat{E}_i)\pm P_{\rm II}^{+}B_1(\hat{E}_i)+A_{\rm II}^{+}B_2(\hat{E}_i)}{B_0(\hat{E}_i)\pm P_{\rm II}^{-}B_1(\hat{E}_i)+A_{\rm II}^{-}B_2(\hat{E}_i)}\times\frac{B_0(\hat{E}_i)\pm P_{\rm V}^{+}B_1(\hat{E}_i)+A_{\rm V}^{+}B_2(\hat{E}_i)}{B_0(\hat{E}_i)\pm P_{\rm V}^{-}B_1(\hat{E}_i)+A_{\rm V}^{-}B_2(\hat{E}_i)}\right]_{U\mathrm{or}D}, \tag{12}$$

where $T^{\pm}$ and $T^{\mp}$ are the possible time dependent asymmetry in the β-ray counting in $A_M^{\pm}$ and $A_M^{\mp}$ cycles caused by the intensity fluctuation of the incident beam, $N_{\rm i}^{\pm}$ are the β-ray counting from the positive $+$ and the negative $-$ alignment in counting Sec. I in the main sequence program and the upper and lower signs are for up and down counters, respectively. Here it should be noted that in Eq. (12) the time dependent asymmetry $T^{\pm}$ and $T^{\mp}$ are completely canceled out. Neglecting higher order contributions from the alignment and the residual polarization, the alignment correlation term is ideally given by

$$\left[\frac{B_2(\hat{E}_i)}{B_0(\hat{E}_i)}\right]_{U\mathrm{or}D}\cong\frac{R_{U\mathrm{or}D}(\hat{E}_i)-1\mp\Delta P}{\hat{A}}, \tag{13}$$

where $\hat{A}=(A_{\rm II}^{+}-A_{\rm II}^{-})+(A_{\rm V}^{+}-A_{\rm V}^{-})$ is the effective alignment and $\Delta P=(P_{\rm II}^{+}-P_{\rm II}^{-})+(P_{\rm V}^{+}-P_{\rm V}^{-})$ is the residual polarization caused by the imperfect spin manipulation and was negligibly small $|\Delta P/\hat{A}|\leqslant 0.35\%$ as shown in Table I. Moreover, summing the alignment correlation terms obtained from up and down counters the small but finite effects of the residual polarization can be rejected as

$$\frac{B_2(\hat{E}_i)}{B_0(\hat{E}_i)}=\frac{1}{2}\left(\left[\frac{B_2(\hat{E}_i)}{B_0(\hat{E}_i)}\right]_U+\left[\frac{B_2(\hat{E}_i)}{B_0(\hat{E}_i)}\right]_D\right)$$
$$\cong\frac{1}{2\hat{A}}[R_U(\hat{E}_i)-1+R_D(\hat{E}_i)-1]. \tag{14}$$

In the actual analysis the higher order contributions from the alignment and the small residual polarization were properly taken into account by directly solving Eq. (12).

B. Systematic corrections and errors

We made some systematic corrections to our experimentally determined alignment correlation terms and evaluated the uncertainties of the corrections considered systematic errors. Correction factors denoted by C_i are defined as

$$\left[\frac{B_2(\hat{E}_j)}{B_0(\hat{E}_j)}\right]_{\rm corr}=\prod_i C_i\times\left[\frac{B_2(\hat{E}_j)}{B_0(\hat{E}_j)}\right]_{\rm uncorr}, \tag{15}$$

where i's are Ω, P, BR, RES, and HD defined below and j ranges from 5 to 13 MeV by 1 MeV step. Since the alignment was deduced from the observed polarization averaged over β-ray energy, corrections to the observed polarization and hence to the alignment are energy independent. Corrections of the alignment correlation terms themselves are energy dependent. The correction factors considered in the present analysis are summarized in Table II. The energy dependent corrections are illustrated in Fig. 8 in solid lines together with the total correction in dotted lines. The effects

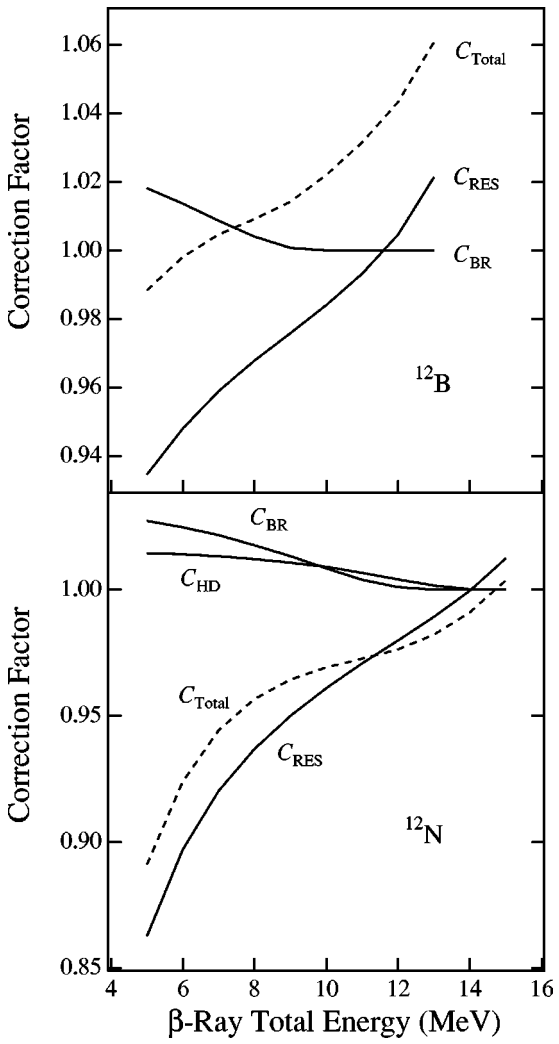

FIG. 8. Energy dependent and total correction factors. The total correction factor is defined in Eq. (15) as $C_{\text{total}}=\Pi_i C_i$. The energy dependent correction factors for ^{12}B (upper) and ^{12}N (lower) are shown in the solid lines as functions of β-ray total energy in the analyzed energy region. The dotted lines are the total correction factors, which include energy independent part. Each correction factors is defined in Sec. IV B.

of the corrections of the alignment correlation terms on $2Mf_T/f_A$ and y can be roughly estimated from the change of the slope of the alignment correlation terms as a function of the β-ray energy (alignment correlation coefficient) as shown in Eq. (5). The systematic errors are also shown in Table II in relative % to the slope. Each correction is explained briefly below.

a. The finite solid angle of the β-ray detectors. The degree of alignment was deduced from the polarization. The polarization term, however, has a different angular distribution from that of the alignment. Since the counter solid angle was finite, the observed polarization is the average of the $P_1(\cos\theta)$ dependence over the present solid angle while the alignment correlation term is the average of $P_2(\cos\theta)$ dependence as shown in Eq. (3). Thus the calculated alignment correlation term has a correction factor $\int P_1(\cos\theta)d\Omega/\int P_2(\cos\theta)d\Omega$. The actual angular distribution, however, suffers from the scattering effect caused by the Mg catcher and thus the distribution is modified. This was taken into account by the EGS4 simulation [19]. The correction factor C_Ω is then given by

$$C_\Omega=\frac{\int\int P_1(\cos\theta)g(\theta,E)S(E)dE\,d\Omega}{\int\int P_2(\cos\theta)g(\theta,E)S(E)dE\,d\Omega}, \tag{16}$$

where $g(\theta,E)$ is the scattering effect of the β rays emitted from the catcher. The correction factor affects the slope of the alignment correlation terms by + 5.38% for ^{12}B and + 5.51% for ^{12}N.

b. β-ray energy dependence of the angular distribution. In the β-ray angular distribution, the polarization term is given by $\mp P(p/E)(B_1/B_0)P_1(\cos\theta)$. Because the factor $(p/E)B_1/B_0$ is slightly deviated from unity, the difference needs to be corrected. The correction factor C_P is energy independent and is given by

$$C_P=\frac{\int\int S(\mu)P(p/E)(B_1/B_0)R(\mu,E)d\mu\,dE}{\int\int S(\mu)R(\mu,E)d\mu\,dE}, \tag{17}$$

where the $R(\mu,E)$ is the counter response function. This factor affects the slope of the alignment correlation terms by -0.21% for ^{12}B and -2.82% for ^{12}N.

c. β-decay branches. The β decays of ^{12}B and ^{12}N have small decay branches to the excited states of ^{12}C. Since the branch to the first excited state has a different maximum β-ray energy and a change of spin $1^+\rightarrow 2^+$ from that of main branch to the ground state, which results in the change of angular distribution, the measured alignment and polarization are distorted due to the small mixture from the branch. The latest branching ratios [20] (1.28 and 1.898 % for ^{12}B and ^{12}N, respectively) were used for the correction. The energy dependent part $C^A_{\text{BR}}(E)$ and energy independent part C^P_{BR} of the correction factors are given by

$$C^A_{\text{BR}}(E)=\left(1-\frac{9}{10}\frac{\int S_1(\mu)R(\mu,E)d\mu}{\int S(\mu)R(\mu,E)d\mu}\right)^{-1},$$

$$C^P_{\text{BR}}=1-\frac{3}{2}\frac{\int S_1(\mu)R(\mu,E)d\mu\,dE}{\int S(\mu)R(\mu,E)d\mu\,dE}, \tag{18}$$

respectively. Here S_1 is the β-ray spectrum of the decay to the first excited state of ^{12}C. These factors affect the slope of the alignment correlation terms by -0.42% for ^{12}B and -1.48% for ^{12}N.

d. Response function of the β-ray detectors. The observed β-ray energy spectrum is distorted from its original statistical shape due to the response of the β-ray counter as discussed above. Because of the response, the alignment effect at the given energy spreads out into another energy region. The correction factor $C_{\rm res}(E)$ for this effect is energy dependent and is given by

$$C_{\rm res}(E)=E\frac{\int S(\mu)R(\mu,E)d\mu}{\int S(\mu)\mu R(\mu,E)d\mu}, \tag{19}$$

which affects the slope of the alignment correlation term by -3.86% for ^{12}B and -4.07% for ^{12}N.

e. Admixture of the HD^+ beam in the ^3He beam. In the production of ^{12}N a small but finite admixture of HD^+ beam produced ^{12}B, to disturb the measured ^{12}N energy spectrum. The HD^+ can be mixed in the ^{3}He beam through the residual H and D atoms on the wall of the ion source and in the canal of the gas inlet forming HD molecules and ionized and accelerated by the Van de Graaff accelerator. Since the mixed HD^+ in ^{3}He beam cannot be separated out by the analyzer magnet, it hit residual ^{11}B in the ^{10}B enriched target (90.4 – 99.8% enrichment) and produced unwanted ^{12}B through the $^{11}B(d,p)^{12}B$ reaction. Due to large cross section of the (d,p) reaction, this contamination can be significant with even a small admixture. This contamination was monitored from the analysis of the β-ray time spectra and the polarization correlation term which is sensitive to the admixture of ^{12}B, to obtain the ratio of the yield of the unwanted ^{12}B to that of ^{12}N to be $1\pm0.5\%$. The energy dependent part $C^A_{\rm HD}(E)$ and energy independent part $C^P_{\rm HD}$ of the correction factors are given by

$$C^A_{\rm HD}(E)=\frac{\int [S(\mu)+S_{\rm mix}(\mu)]d\mu}{\int S(\mu)R(\mu,E)d\mu},$$

$$C^P_{\rm HD}=\frac{\int\int S(\mu)R(\mu,E)d\mu\,dE}{\int\int [S(\mu)+S_{\rm mix}(\mu)]R(\mu,E)d\mu\,dE}, \tag{20}$$

respectively. Here, $S_{\rm mix}$ is the mixed ^{12}B energy spectrum. These factors affect the slope of the alignment correlation terms by -0.25% for ^{12}N.

f. Propagation of the error in the observed alignment. The error in alignment affects evenly all the data points of different energy bins. Although the origin of the effect was statistical, the error was taken into account as a systematic error from the nature of the error.

g. Energy calibration. The energy scale was experimentally determined by producing several β-emitting unstable nuclei and by detecting their end point energies. The nonlinearity of the scale directly affects the slope of the alignment correlation term but the sensitivity of the present procedure to the nonlinearity is limited. The possible effect within the present sensitivity was taken into account as a systematic error.

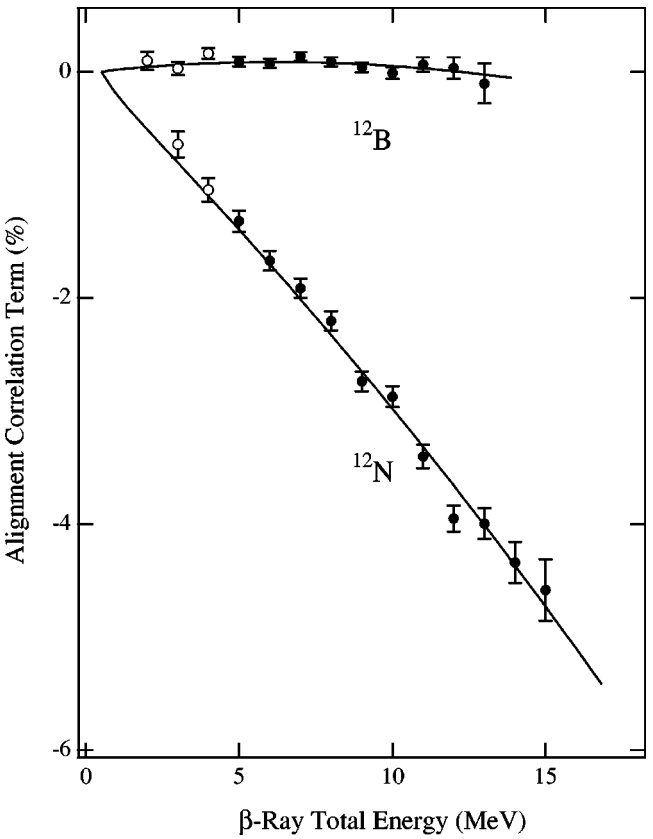

FIG. 9. Alignment correlation terms of ^{12}B and ^{12}N. The corrected alignment correlation terms of ^{12}B and ^{12}N are shown as functions of β-ray total energy. The full circles are the data used in the extraction of the final result. The solid lines are the theoretical curves best fit to the present data. $\chi^2/\nu=1.02$ was obtained.

h. Incident beam position on the target. The change in incident beam position on the target resulted in a slight change in the distribution of the recoiling nucleus on the surface of the catcher. The β-ray scattering effect and the energy loss in the catcher depends on that distribution and thus is affected by the beam position changes. This effect was evaluated by the EGS4 simulation and taken into account as a systematic error.

i. Catcher thickness. As previously described, the Mg catcher was etched every 72 h because of the gradual decrease in the polarization due to the contamination on the surface of the catcher. Each time the Mg catcher was etched its decrease in thickness affected, i.e., reduced the β-ray scattering effect and the energy loss in the catcher. The effect was evaluated by the EGS4 simulation and taken into account as a systematic error.

V. RESULT AND DISCUSSION

The alignment correlation terms were obtained as a function of the β-ray total energy as shown in Fig. 9 after the careful consideration of the corrections and errors. In this

TABLE III. Result of the theoretical curve best fits to the data. The results of the data obtained in the present study and 1996 are summarized. Errors are evaluated at a 90% C.L. and all the values are in units of $1/2M$. The asymmetry in the axial charge $\Delta y = 0.10 \pm 0.05$ was used.

Year	$2Mf_T/f_A$	Error			Year	y	Error	
		stat.	syst.	theory			stat.	syst.
Without Δy					Present	4.96	0.09	0.05
Present	-0.31	0.09	0.07		1996	4.65	0.17	0.14
1996	-0.02	0.17	0.15					
					Mean	4.90		0.10
With Δy								
Present	-0.21	0.09	0.07	0.05				
1996	$+0.08$	0.17	0.15	0.05				
Mean	-0.15		0.12	0.05				

figure the full circles are the present alignment correlation terms used in the extraction of the final result and the open circles at low β-ray energy are not. The solid lines are the theoretical curves best fit to the data as discussed below.

A. Result of our present study

In order to determine precisely the axial charge from the alignment correlation term, higher order effects had to be taken into consideration as stated in Sec. II B. For this purpose we adopted a formulation of the angular distribution which makes it possible to introduce higher order partial waves for leptons, Coulomb corrections for the finite size of nuclei and radiative corrections [10,11]. Using the full formula, we have made a least χ^2 fit of the theoretical curves simultaneously to a set of ^{12}B and ^{12}N data resulting in slightly curved lines for alignment terms as functions of β-ray energy. The analyzed region of the experimental data was from 4.5 to 13.5 MeV (data points of 5–13 MeV in Fig. 9) for ^{12}B and 4.5 to 15.5 MeV (data points of 5–15 MeV in Fig. 9) for ^{12}N in β-ray total energy. The free parameters for the fit were the axial charge y and the induced tensor term f_T as shown in Eqs. (5) and (6). To extract f_T we used a value for the experimental weak magnetism of $2Ma = 4.04 \pm 0.03$, which was determined [17] from all the available data pertaining to the transition strength of the $M1$-γ decay from the 15.11 MeV excited state in ^{12}C [21], $\Gamma_\gamma = (38.2 \pm 0.6)$ eV. From the fit of the theoretical curves to the experimental data, we obtain the results listed in Table III, where we had the reduced χ^2 minimum $\chi^2/\nu = 1.02$, ν being the degree of freedom of the fit. We have the axial charge from the present data as

$$y = 4.96 \pm 0.09 \ \text{(stat.)} \pm 0.05 \ \text{(syst.)}, \tag{21}$$

at a 90% confidence level (C.L.) and $2Mf_T/f_A = -0.21 \pm 0.09$ (stat.) ± 0.07 (syst.) ± 0.05 (theory) [17], where the asymmetry in the axial charges $\Delta y = 0.10 \pm 0.05$ has been taken into account. This result is consistent with but more precise than previous result [4].

B. Combined result of the present and 1996 studies

To combine the present result with the previous one obtained in 1996 [4], we applied newly studied systematic corrections to the alignment correlation terms obtained in 1996 and considered systematic errors. We did not include results obtained before 1996 because they have large systematic errors resulted from the counter response and from the unknown hyperfine interaction in Mg catcher at that time. The main part of the reanalysis of the systematic correction was made in the β-ray scattering effect in the Mg catcher, which affects the correction of the counter solid angle. The correction factor $C_\Omega = 1.031$ for the alignment correlation terms was replaced by 1.054 for ^{12}B and by 1.055 for ^{12}N. As a result from the data obtained in 1996 we have

$$y = 4.65 \pm 0.17 \ \text{(stat.)} \pm 0.14 \ \text{(syst.)}, \tag{22}$$

at a 90% C.L., where the systematic errors due to the β-ray scattering was added which turned out to be small relative to the original one. Finally, combining the 1996 and the present results we have

$$y = 4.90 \pm 0.10, \tag{23}$$

at a 90% C.L. Here the quadratic sum of the statistical and the systematic errors was used for the weight of the sum.

C. Soft-π theorem

According to the theoretical work [11,22] the impulse value which includes the core-polarization effect is evaluated to be $y_{\text{IA}} = 2.85$ and the soft-π contribution $y_{\text{soft-}\pi} = 1.30$ using the Hauge-Maripuu model [23]. The core-polarization effect was calculated in the $(0+2)\hbar\omega$ configuration space to be -0.32 ± 0.03 by use of the M3Y interaction [24], the strength of which is consistent with the one obtained in the analysis of the magnetic form factor in the inelastic scattering of electrons on ^{12}C. Thus, the total theoretical axial charge reaches

$$y_{\text{theor}} = y_{\text{IA}} + y_{\text{soft}-\pi} = 4.15, \tag{24}$$

which corresponds to an enhancement of 46% relative to the y_{IA} value. This predicted value is still 26% less than the present experimental enhancement of 72%.

D. Heavy meson contribution

The exchange current effect based on short range correlations of heavy mesons (σ, ω, and ρ) in the mass $A = 12$ triad was evaluated by Koshigiri *et al.* [22] using the hard-π model [8,9] for the ρ-π diagrams with the Hauge-Maripuu model [23]. They retained only the pair currents which involve the scalar meson (σ) and the exchange of vector mesons (ω and ρ) up to $O(1/M^2)$. The exchange current operators and related parameters were essentially the same as

TABLE IV. Enhancement of the axial charge by the heavy mesons [22]. The Bonn potential parameter adopted in the Kirchbach's paper [8] is used for model A and model B corresponds to another set of Bonn potential in the configuration space [25].

Meson	$y_{\text{hard-}\pi}$			
	Model A		Model B	
	no src	src	no src	src
$\pi-\rho$	0.843	0.853	0.593	0.602
σ	0.304	0.219	0.323	0.231
ω	0.355	0.266	0.352	0.266
ρ	-0.016	0.019	0.101	0.086
$\sigma+\omega+\rho$	0.643	0.504	0.777	0.583
Total	1.487	1.357	1.369	1.186

those used by Kirchbach *et al.* [24]. The numerical values summarized in Table IV give the contribution of the exchange current to the axial charge matrix element. In the table two types of calculations based on different models are listed and the values without short range correlation are also tabulated for comparison. For model *A* the Bonn potential parameters in the Kirchbach *et al.* [8] are adopted in the configuration space [25]. Model *B* uses another set of the Bonn potential parameters. Since both values are close to the soft-π value of 1.30 given above, we may take the mean value $y_{\text{hard-}\pi}=1.27$ as the theoretical value for the mesonic effect. We assume an uncertainty of ± 0.17 that is twice as much as the difference of these two predictions. Finally, we have the total theoretical axial charge as

$$y_{\text{theor}}=y_{\text{IA}}+y_{\text{hard-}\pi}=4.12\pm 0.17, \tag{25}$$

which is inconsistent with the experimental value $y=4.90\pm 0.10$. A better agreement between theory and experiment might be obtained by introducing still higher order exchange current terms.

E. In-medium mass renormalization

In 1991, Warburton *et al.* systematically analyzed the first-forbidden β-decay rates of the nuclei in the lead region and shown that the axial charges are enhanced by 80% relative to the IA values. This is about twice that obtained from the calculation based on soft π exchange currents. The large enhancement in the Pb region may show its dependence on mass around the β-decaying nuclei. To explain the large enhancement, they proposed in-medium renormalizations of the nucleon mass [6] which are also theoretically discussed in the framework of chiral perturbation theory [26,27]. The experimental excess of about 26% over the theoretical value $y_{\text{th}}\sim 4.15$ might be also accounted for by the baryonic scaling in a nuclear medium. According to the in-medium renormalization of hadron masses [26], the nucleon mass should be reduced as

$$\frac{m_{\text{N}}^*}{m_{\text{N}}}\approx\frac{m_\sigma^*}{m_\sigma}\approx\frac{m_\rho^*}{m_\rho}\approx\frac{m_\omega^*}{m_\omega}\approx\frac{f_\pi^*}{f_\pi}=\Phi(\rho), \tag{26}$$

where m_{N}, m_σ, m_ρ, and m_ω are the masses of the hadrons and f_π is the π decay constant. Here the asterisks refer to the renormalized values in the nuclear medium. The enhancement factor defined by Warburton is written as

$$\varepsilon_{\text{MEC}}=\frac{M_1^*+M_2^*}{M_1}=\frac{1}{\Phi(\rho)}\left(1+\frac{M_2}{M_1}\right), \tag{27}$$

with $M_i^*=M_i/\Phi(\rho)$, where M_1^* is the in-medium single-particle axial-charge matrix element (IA) and M_2^* is the in-medium exchange current matrix element and the values of M_i without an asterisk are calculated with $\Phi(\rho)=1$. In the mass $A=12$ triad with the experimental enhancement, $\varepsilon_{\text{MEC}}=1.72\pm 0.04$ and the theoretical ratio of $M_2/M_1=0.45\pm 0.06$, we have

$$\Phi(A=12)=0.84\pm 0.04. \tag{28}$$

Thus, in the present framework the nucleons decaying in ^{12}B (^{12}N) are $(16\pm 4)\%$ lighter than the free nucleon mass. To check consistency with other systems, we have the ε_{MEC} value for the Pb region where the observed enhancements were fairly well accounted for by the IA values plus the exchange current effects [9]. The amount left unexplained, less than 25% of the experimental enhancement, can be attributed to in-medium renormalization [26]. The experimental value of $\varepsilon_{\text{MEC}}=1.79\pm 0.04$ [28] and the theoretical ratio $M_2/M_1=0.5\pm 0.1$, which is quite insensitive to the details of the nuclear models and also to nuclear masses [29], gives $\Phi(A=208)=0.84\pm 0.06$, leading to a mass reduction relative to the free nucleon mass of $(16\pm 6)\%$ for the nucleons decaying in the nuclei in the Pb region. Also if we apply the same analysis for ε_{MEC} obtained from the first forbidden β-decay rates in other nuclear masses using the value of M_2/M_1 given above [29], the enhancement factor of $\varepsilon_{\text{MEC}}=1.61\pm 0.03$ [28] in the mass $A=16$ region suggests a nucleon mass reduction of $(7\pm 6)\%$, $\varepsilon_{\text{MEC}}=1.7\pm 0.1$ [30] in the mass $A=18$ region gives $(13\pm 8)\%$, $\varepsilon_{\text{MEC}}=1.52\pm 0.07$ [31] in the mass $A=50$ region gives $(1\pm 8)\%$, $\varepsilon_{\text{MEC}}=1.8\pm 0.3$ [32] in the mass $A=96$ region gives $(14\pm 16)\%$ and in the mass $A=132$ region $\varepsilon_{\text{MEC}}=1.82\pm 0.07$ [33] gives $(18\pm 6)\%$ mass reduction. Such mass renormalizations are also phenomenologically in agreement with the ones evaluated from magnetic moments. A renormalization of about 3% was found [34] for nuclei with the mass $A=16\pm 1$ and 40 ± 1 which have one nucleon added to or removed from the doubly closed shell nuclei. The renormalized unit of the magnetic moment, the nuclear magneton μ_{N}, was extracted from their isoscalar magnetic moments. Also, a mass reduction of $(8\pm 3)\%$ was extracted by Yamazaki [35] from the anomalous orbital g factors of the nuclei in the Pb region. The nuclear mass dependence of the mass renormalization is illustrated in Fig. 10. Apparently, the mass reduction of about 10% can be seen throughout a wide range of nuclear masses, although the error bars are relatively large. We need even more precision and data points to reveal the mass dependence of the nuclear medium effects on mass renormalization.

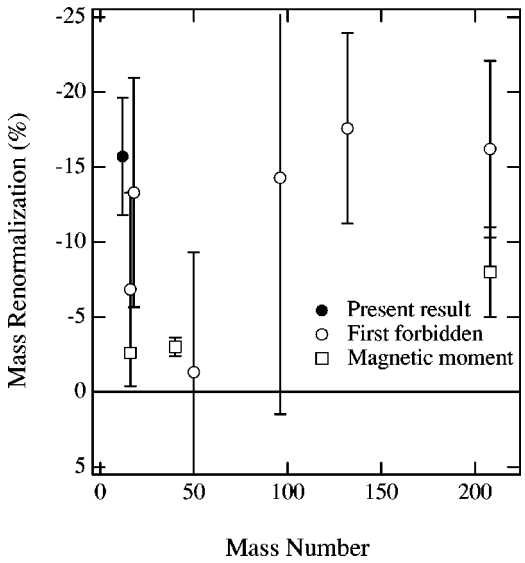

FIG. 10. Mass renormalization. For the extraction of Φ, the value $M_1/M_2=0.5\pm0.1$ [29] was consistently used. The full circle is the present result, the open circles are from the result of the first forbidden β decays in several nuclear mass and the open squares are the result from the isoscaler magnetic moments.

VI. CONCLUSION

The alignment correlation terms in the β-ray angular distributions from the purely spin aligned ^{12}B and ^{12}N have been accurately measured to detect the axial charge in the main axial vector current. We have the axial charge as $y=4.96\pm0.09$ (stat.) ±0.05 (syst.) at a 90% C.L., which is consistent with but more reliable than the previous results. If we combine the present result with the previous one obtained in 1996, the corrections of which were newly considered and applied, we have $y=4.90\pm0.10$ at a 90% C.L., which shows as much as (72 ± 4)% experimental enhancement relative to the IA value $y_{\mathrm{IA}}=2.85$. The result can be fairly well explained by the theoretical calculation that includes the IA value, the core polarization effect and the soft-π contribution $y_{\mathrm{th}}=4.15$ which shows 46% enhancement. There is, however, still 26% difference between the experimental enhancement and theoretical values. The heavy-meson exchange effect with the IA value does not account for the difference, either. If we introduce the in-medium renormalization of hadron masses, the experimental excess suggests an in-medium nucleon-mass reduction of (16 ± 4)% at the place where the decaying nucleon resides for the mass $A=12$ triad.

ACKNOWLEDGMENTS

We would like to express our sincere thanks to M. Morita at Josai International University and G. F. Krebs at Lawrence Berkeley National Laboratory for their valuable discussions. We also would like to thank the crew of the Van de Graaff Laboratory of Osaka University, M. Sakamoto, T. Sakurai, and K. Ohsawa. The present work was supported in part by the Japan Society for the Promotion of Science for Young Scientists and by the Grant in Aid for Scientific Research from the Ministry of Education, Culture and Science, Japan and also by the Yamada Science Foundation.

[1] K. Kubodera, J. Delorme, and M. Rho, Phys. Rev. Lett. **40**, 755 (1978).

[2] J. Delorme, Nucl. Phys. **A374**, 541c (1982).

[3] Y. Masuda, T. Minamisono, Y. Nojiri, and K. Sugimoto, Phys. Rev. Lett. **43**, 1083 (1979); T. Minamisono, K. Matsuta, Y. Nojiri, and K. Takeyama, J. Phys. Soc. Jpn. Suppl. **55**, 382 (1986); T. Minamisono, A. Kitagawa, K. Matsuta, and Y. Nojiri, Hyperfine Interact. **78**, 77 (1993).

[4] T. Minamisono, K. Matsuta, T. Yamaguchi, K. Minamisono, M. Fukuda, A. Kitagawa, and K. Koshigiri, Phys. Rev. Lett. **82**, 1644 (1999).

[5] J-I. Fujita and M. Ichimura, in *Mesons in Nuclei*, edited by M. Rho and D. H. Wilkinson (North-Holland, Amsterdam, 1979), p. 625; T. Yamazaki, *ibid.*, p. 651; A. Arima and H. Hyuga, *ibid.*, p. 683; B. H. Wildenthal and W. Chung, *ibid.*, p. 721; D. O. Riska, *ibid.*, p. 755; A. Arima, K. Shimizu, W. Benzu, and H. Hyuga, Adv. Nucl. Phys. **18**, 1 (1987); I. S. Towner, Phys. Rep. **155**, 263 (1987).

[6] E. K. Warburton, Phys. Rev. Lett. **66**, 1823 (1991); E. K. Warburton, I. S. Towner, and B. A. Brown, Phys. Rev. C **49**, 824 (1994); E. K. Warburton and I. S. Towner, Phys. Lett. B **294**, 381 (1994).

[7] C. A. Gagliardi, G. T. Garvey, J. R. Wrobel, and S. J. Freedman, Phys. Rev. Lett. **48**, 914 (1982); L. A. Hamel, L. Lessard, H. Jeremie, and J. Chauvin, Z. Phys. A **321**, 439 (1985); T. Minamisono, K. Takeyama, T. Ishigai, H. Takeshima, Y. Nojiri, and K. Asahi, Phys. Lett. **130B**, 1 (1983); M. Mihara, M. Fukuda, A. Harada, T. Fukao, M. Saito, A. Matsumoto, K. Matsuta, Y. Nojiri, and T. Minamisono, in *Non Nucleonic Degrees of Freedom Detected in Nucleus*, edited by T. Minamisono, Y. Nojiri, T. Sato, and K. Matsuta (Word Scientific, Singapore, 1996), p. 224.

[8] E. Ivanov and E. Truhlik, Nucl. Phys. **A316**, 437 (1979); S. Chechanowicz and E. Truhlik, *ibid.* **A414**, 508 (1984); J. Adam and E. Truhlik, J. Phys. B **33**, 558 (1983); **34**, 1157 (1984); J. Adam, Ch. Hajduk, H. Henning, P. U. Sauer, and E. Truhlik, Nucl. Phys. **A531**, 623 (1991); M. Kirchbach, S. Kamalov, and H.-U. Jager, Phys. Lett. **144B**, 319 (1984); H.-U. Jager, M. Kirchbach, and E. Truhlik, Nucl. Phys. **A404**, 456 (1983); V. I. Ogievesky and B. M. Zupnik, Nucl. Phys. **B24**, 612 (1970); M. Kirchbach, D. O. Riska, and K. Tsushima, Nucl. Phys. **A542**, 616 (1992).

[9] I. S. Towner, Nucl. Phys. **A542**, 631 (1992); E. K. Warburton and I. S. Towner, Phys. Rep. **242**, 103 (1994).

[10] M. Morita, M. Nishimura, A. Shimizu, H. Ohtsubo, and K. Kubodera, Prog. Theor. Phys. Suppl. **60**, 1 (1976); M. Morita, *Beta Decay and Muon Capture* (W. A. Benjamin, New York, 1973).

[11] M. Morita, M. Nishimura, and H. Ohtsubo, Phys. Lett. **73B**, 17 (1977); K. Koshigiri, H. Ohtsubo, and M. Morita, Prog. Theor.

Phys. **66**, 358 (1981); M. Morita, R. Morita, and K. Koshigiri, Nucl. Phys. **A577**, 387c (1994).
[12] M. Morita, in *Non Nucleonic Degrees of Freedom Detected in Nucleus*, edited by T. Minamisono, Y. Nojiri, T. Sato, and K. Matsuta (Word Scientific, Singapore, 1996), p. 125.
[13] K. Koshigiri, M. Nishimura, H. Ohtsubo, and M. Morita, Nucl. Phys. **A319**, 301 (1979).
[14] Y. Yokoo and M. Morita, Prog. Theor. Phys. Suppl. **60**, 37 (1976).
[15] K. Koshigiri, M. Nishimura, H. Ohtsubo, and M. Morita, Nucl. Phys. **A319**, 301 (1979); K. Koshigiri, H. Ohtsubo, and M. Morita, J. Phys. Soc. Jpn. Suppl. **55**, 1014 (1986).
[16] T. Minamisono, K. Matsuta, T. Yamaguchi, K. Minamisono, T. Ikeda, Y. Muramoto, M. Fukuda, Y. Nojiri, A. Kitagawa, K. Koshigiri, and M. Morita, Phys. Rev. Lett. **80**, 4132 (1998).
[17] K. Minamisono, K. Matsuta, T. Minamisono, T. Yamaguchi, T. Sumikama, T. Nagatomo, M. Ogura, T. Iwakoshi, M. Fukuda, M. Mihara, K. Koshigiri, and M. Morita, Phys. Rev. C (to be published).
[18] A. Kitagawa, K. Matsuta, Y. Nojiri, and T. Minamisono, Hyperfine Interact. **60**, 869 (1990).
[19] W. R. Nelson, H. Hirayama, and D. W. O. Rogers, Stanford University Report No. SLAC-265.
[20] F. Ajzenberg-Selove, Nucl. Phys. **A506**, 1 (1990).
[21] P. M. Endt, Nucl. Phys. **114**, 48 (1968); **114**, 69 (1968); B. T. Chertok, C. Sheffield, J. W. Jightbody, Jr., S. Penner, and D. Blum, Phys. Rev. C **8**, 23 (1973); U. Deutschmann, G. Lahm, and R. Neuhausen, Nucl. Phys. **A411**, 337 (1983).
[22] K. Koshigiri, R. Morita, and M. Morita, in *Weak and Electromagnetic Interactions in Nuclei*, edited by H. Ejiri, T. Kishimoto, and T. Sato (World Scientific, Singapore, 1995), p. 361; K. Koshigiri, H. Ohtsubo, K. Kubodera, and M. Morita, in *Nuclear Weak Process and Nuclear Structure*, edited by M. Morita, H. Ejiri, H. Ohtsubo, and T. Sato (World Scientific, Singapore, 1989), p. 52.
[23] P. S. Hauge and S. Maripuu, Phys. Rev. C **8**, 1609 (1973).
[24] G. Bertsch, J. Borysowicz, H. Mcmanus, and W. G. Love, Nucl. Phys. **A284**, 399 (1977).
[25] R. Machleidt, Adv. Nucl. Phys. **19**, 189 (1989).
[26] Tae-Sun Park, I. S. Toner, and K. Kubodera, Nucl. Phys. **A579**, 381 (1994).
[27] G. E. Brown and M. Rho, Phys. Rev. Lett. **66**, 2720 (1991).
[28] E. K. Warburton, I. S. Towner, and B. A. Brown, Phys. Rev. C **49**, 824 (1994).
[29] K. Kubodera and M. Rho, Phys. Rev. Lett. **67**, 3479 (1991).
[30] E. G. Adelberger, M. M. Hindi, C. D. Hoyle, H. E. Swanson, R. D. Von Lintig, and W. C. Haxton, Phys. Rev. C **27**, 2833 (1983).
[31] E. K. Warburton, Phys. Rev. C **44**, 233 (1991).
[32] H. Mach, E. K. Warburton, R. L. Gill, R. F. Casten, J. A. Becker, B. A. Brown, and J. A. Winger, Phys. Rev. C **41**, 226 (1990).
[33] E. K. Warburton and I. S. Towner, Phys. Lett. B **294**, 1 (1992).
[34] T. Minamisono, Y. Nojiri, K. Matsuta, K. Takeyama, A. Kitagawa, T. Ohtsubo, A. Ozawa, and M. Izumi, Nucl. Phys. **A516**, 365 (1990); T. Minamisono, T. Ohtsubo, Y. Nakayama, T. Araki, K. Mashitani, K. Matsuda, E. Takahashi, M. Tanigaki, Y. Someda, M. Tanaka, A. Kitagawa, M. Fukuda, K. Matsuta, and Y. Nojiri, Hyperfine Interact. **73**, 347 (1992).
[35] T. Yamazaki, Phys. Lett. **160B**, 227 (1985).